ANALYSIS OF AN AIR SOURCE HEAT PUMP SYSTEM WITH SPEED CONTROLLED COMPRESSOR AND VAPOR INJECTION

***Franz Hengel**, Dipl.-Ing. B.Sc., Research Assistant*
***Andreas Heinz**, Dipl.-Ing. (FH) Dr.techn., Project-Senior Scientist*
***René Rieberer**, Ao.Univ.-Prof. Dipl.-Ing. Dr.techn., Deputy Head of the Institute*
Graz University of Technology, Institute of Thermal Engineering,
Inffeldgasse 25/B, 8010 Graz, Austria

Abstract: The thermal output of an air source heat pump (ASHP) with constant speed compressor increases at increasing ambient air temperature while the heating demand of the building decreases. Consequently, the thermal output of the heat pump is much higher than the actual demand for a large part of the year. Speed controlled compressors (VSD) offer the possibility to adapt the thermal capacity of the heat pump to the current load with the advantages of continuous operation, lower start and stop losses and higher efficiency.

At low ambient air temperatures and especially with heating systems that require high flow temperatures ASHP are operated with high pressure ratios and therefore achieve relatively poor efficiencies. Additionally, the heating capacity decreases and the compressor discharge temperature increases to very high values at low evaporation temperatures. In order to improve ASHP systems enhanced vapor injection (EVI) systems are one possibility. By means of a vapor injection into the compressor at an intermediate pressure the compressor discharge temperature can be reduced and both the heating capacity and the COP of the heat pump can be increased at low evaporation temperatures.

In this work a heat pump system comprising a speed controlled compressor and an EVI cycle (CEV) is analyzed by means of detailed measurements in the laboratory. The measured data is used to parameterize and validate a detailed simulation model of the heat pump. Using this model, dynamic system simulations are performed to analyze the seasonal performance factor (SPF) of the heat pump system in comparison to a standard heat pump (CSD).

Key Words: heat pump, R410A, economizer-cycle, variable speed drive, TRNSYS

1 INTRODUCTION

Conventional heat pumps are usually equipped with a constant-speed compressor, which is operated in on/off-mode to provide the energy that is necessary e.g. for space heating. Especially with ASHPs the thermal output increases at an increasing ambient air temperature, while the required heating capacity of the building decreases. Consequently the thermal output of the heat pump is much higher than the actual demand for the major part of the year causing a large number of on/off cycles of the heat pump.

A heat pump with VSD can adjust its heating capacity to the currently required heating load for a large part of the heating season. This results in a reduction of the number of on/off cycles and an increased efficiency. Different researchers showed the potential of saving electric energy by using a VSD (e.g. Aprea et al., 2004 and Gasser et al., 2008).

ASHP's are widely used in residential heating and cooling systems due to their low installation costs and their effectiveness (Heo et al. 2011). At low ambient air temperatures and especially with heating systems that require high flow temperatures, e.g. retrofit buildings, the heat pump compressor operates at high pressure ratios and therefore the heating system achieves a relatively poor seasonal performance factor (SPF) in cold climates. Other problems are that the heating capacity of ASHP's decreases and that the compressor discharge temperature increases to high values at low ambient temperatures. By means of a vapor injection into the compressor at an intermediate pressure the compressor discharge temperature can be reduced and both the heating capacity and the COP of the heat pump can usually be increased at low evaporation temperatures. Liegeois and Winandy (2008) and Bertsch and Groll (2008) showed higher efficiencies by using an EVI system.

In this work a heat pump system equipped with a speed controlled compressor and a vapor injection cycle is analyzed by detailed measurements in the laboratory. The measured data is used to parameterize and validate a simulation model of the heat pump with an economizer cycle (plate heat exchanger) for EVI and a speed controlled compressor (CEV). Using this model, annual dynamic system simulations for a retrofit building with high flow temperatures for the heating system are performed to analyze the SPF of the heat pump system in comparison to a "standard" single stage heat pump cycle (CSD).

2 BOUNDARY CONDITIONS AND MODELING

This chapter describes the modeling of the hydronic system, which was considered for the simulations as well as the system boundary conditions, climate, building and hot water profile as well as the modeling of the heat pump system and information about the considered compressors.

2.1 Hydronic system modeling

Figure 1 shows the hydronic scheme (adapted from Afjei et al. 2002) for the dynamic system simulation. The system was chosen due to suggestion from Afjei et al. (2002), who have investigated different hydronic systems equipped with heat pumps. On the left side there is the heat pump (HP) and on the right side of the HP the hydronic system with the domestic hot water (DHW) storage and the heating system for the building, which works alternatively. This means that either DHW preparation is done or space heating.

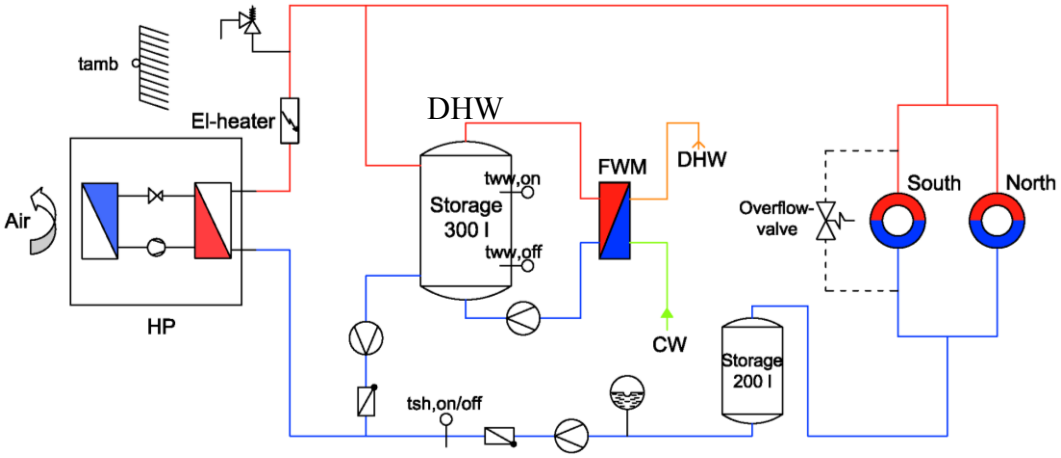

Figure 1: Hydronic scheme adapted from STASCH IV (Afjei et al. 2002)

The building is split into two thermal zones, one on the north and one on the south side of the building. A room temperature control with a thermostatic valve is installed in the southern zone to account for possible solar radiation gains. The overflow valve, which is located in parallel to the thermostatic valve and the space heating system (radiators), ensures that the mass flow rate in the south zone is at least 50 % of the nominal mass flow rate, in order to prevent too high condensation temperatures of the heat pump due to a too low mass flow rate through the condenser. The 200 liter storage in the return line is necessary to increase the runtime of the heat pump, especially in cases of a heat pump with constant-speed compressor, and to reduce the condensation temperature due to the heat storage capacity which ensures lower inlet temperatures to the condenser.

The DHW circuit consists of the heat pump, a 300 liter DHW storage, a pump and a fresh water module (FWM), where the cold water (CW) is heated up, and another circulation pump on the secondary side. Preparing DHW is done (heat pump is on) if the temperature $t_{ww,on}$ is lower than a set point (49 °C) and switches off if the temperature at $t_{ww,off}$ is higher than a set point (53 °C). With simultaneous demand for DHW and space heating, priority is given to DHW. In case of space heating demand the heat pump is switched on or off if following conditions are met for both systems, CEV and CSD.

HP switches on: $t_{sh,on/off} \leq t_{set,rt} - 3\ K$
HP switches off: $t_{sh,on/off} \geq t_{set,rt} + 1\ K$

$t_{set,rt}$ is the temperature set point at the return line obtained from the heating curve (depending on ambient temperature). The electrical power of the circulation pump depends on the mass flow rate and its nominal electric power is 15 W (high efficiency pumps).

2.2 Boundary conditions climate and building

Table 1 provides information about the considered climate and building. For the climate a test reference year (TRY) for Zurich is chosen with a design ambient air temperature of -10 °C and heating degree days of 3406 Kd/a. The assumed building is an adaption of the IEA SHC TASK 44/HPP ANNEX 38 (T44A38) reference building, which has got a heating demand of 100 kWh/(m²·a) for the climate Strasbourg. The reason for this building with high heating demand is that there are still a lot of retrofit buildings available and it is interesting for an EVI cycle because of the higher pressure ratios, where an EVI cycle has got its advantages compared to a standard heat pump. With an indoor temperature of 20 °C the overall heating load of the considered retrofit building is 7.87 kW, which is split in a heating load for the thermal zone in the north with 3.63 kW and 4.24 kW for the zone in the south. The supply temperature of the radiator heating system is 55 °C and the return temperature is 45 °C at design ambient conditions. The higher heating demand of the building in Table 1 (154 kWh/(m²·a)), compared to the T44A38 reference building, can be explained by the different location, the control strategy of the space heating loop (compare chapter 2.1) and the penalty function, which ensures the comfort for space heating. To satisfy this comfort level the penalty function must not exceed 1 % of the space heating demand (Streicher and Heimrath, 2003). Due to this restriction the averaged room temperature of the building in the heating season for the north zone is 21.65 °C and for the south zone 21.34 °C. Hence the heating demand is higher for the north zone compared to the sourth zone.

For the hot water load profile, a data set from the EU Project MacSheep is used (Bales et al. 2012). The DHW heat demand at a temperature difference of 35 K (45 °C DHW temperature and 10 °C cold water temperature) is 3038 kWh/a. Same as for the space heating system a penalty function is implemented which must not exceed 1 % of the DHW demand.

Table 1: Climate and building definition

Climate			Building				
Location	Design temperature [°C]	Heating degree days [Kd/a]	Heating system	Heating demand [kWh/(m²·a)]	Heating load [kW]	Heating area [m²]	Design room temperature [°C]
Zurich	-10	3406	Radiator system	154	7.87	140	20

2.3 Heat pump model

The simulation was performed by means of dynamic system simulations in TRNSYS (TRNSYS 2012) using the semi-physical heat pump model Type 887 (Heinz and Haller 2012). The model is based on a calculation of the thermodynamic refrigerant cycle using the thermodynamic properties of the refrigerant, which are approximated by means of polynomials. The model allows the use of an economizer cycle with a plate heat exchanger or with a “flash tank”. The modeling of the compressor efficiency can be done either with a performance map or with an approach that uses the overall isentropic efficiency $\eta_{is,over}$ and the volumetric efficiency η_{vol}. The heat exchangers are modeled by means of manufacturer data using the conditions on the inlet of the heat exchanger (mass flow rate, pressure, temperature) as well as the UA-Values.

Figure 2 shows a standard heat pump cycle (left side) and a heat pump using an economizer cycle with heat exchanger (right side) in a temperature-enthalpy diagram. It can be seen that the compressor discharge temperature is lowered as well as the condenser capacity and the coefficient of performance can be increased by using an economizer cycle compared to the standard heat pump cycle at high pressure ratios.

For the single stage heat pump (CSD) the compressor is modeled using the performance map from a manufacturer and for the speed controlled heat pump with economizer (CEV) the approach based on $\eta_{is,over}$ and η_{vol} is considered. The necessary data for the CEV was derived from measurements with a test rig (compare chapter 3) in form of polynomials for $\eta_{is,over}$ and η_{vol} as a function of the evaporation temperature t_{evap}, condensation temperature t_{cond} and the compressor speed n_{comp}. Further information referring to this topic will be given in chapter 3.

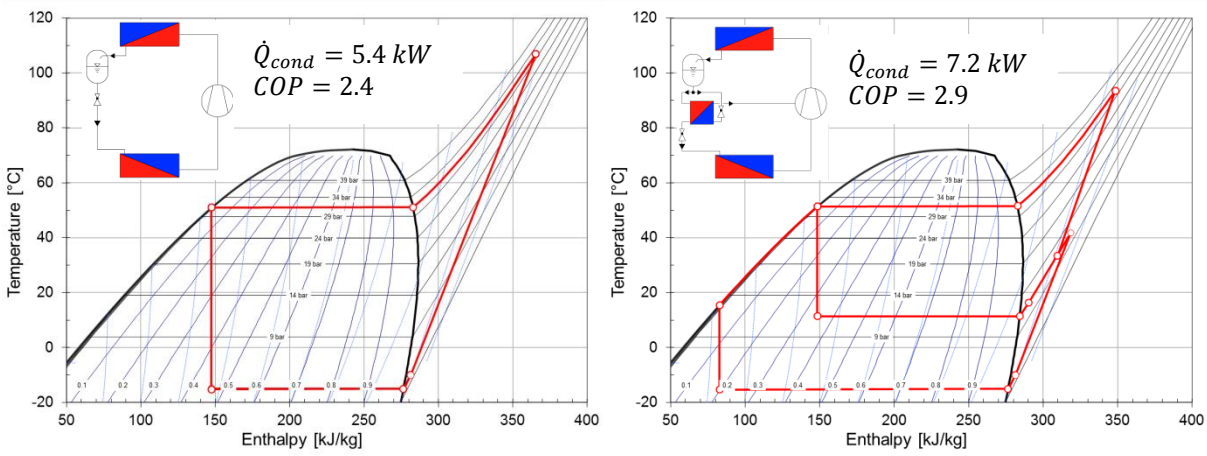

Figure 2: Standard heat pump cycle (left) and economizer cycle (right) in a temperature-enthalpy diagram of R410A

Due to the relatively high variation of the mass flow rate through the refrigerant cycle, a polynomial for the UA-values of the heat exchangers was created. For the condenser the UA-value depends on the mass flow rate on the refrigerant side, the mass flow rate on the heat sink side as well as on the refrigerant temperature at the inlet of the heat exchanger. The UA-value for the evaporator depends just on the mass flow rates (refrigerant side and source side). These polynomials are based on manufacturer data (SWEP 2014) and are used as inputs for the heat pump model.

The electrical power consumption of the fan of the evaporator is also based on manufacturer data. Due to different heating capacities of the considered heat pump and the heat pump, from which the data was taken, a scaling factor is implemented. The nominal electrical power consumption of the fan is 120 W at a speed of 650 rpm below an ambient temperature of 15 °C. The speed of the fan is only reduced linearly above 15 °C in order to stay within the compressor operational limits (max. evaporation temperature) and to ensure that the evaporation temperature will not be decreased by reducing the fan speed. The compressor speed and thus the heating capacity of the heat pump is controlled in a way to reach a set point for the flow temperature at the outlet of the condenser. This set point is calculated by means of the heating curve of the building and the current ambient temperature.

A simplification of the heat pump model is that the heat losses of the refrigerant cycle (except the heat losses of the compressor) as well as the pressure drops in pipes and heat exchangers are neglected. The start and stop losses are calculated in a simplified way (Heinz and Haller, 2012). The defrosting losses are also considered. Depending on the evaporation temperature and the temperature and humidity of the ambient air, a growth of ice on the evaporator is estimated. The estimated heating capacity, which is necessary for melting the ice on the evaporator, is subtracted from the capacity of the condenser, thus reducing the COP. The dynamics of the defrosting process are not considered (Heinz and Haller, 2012).

2.4 Compressor

For the investigations two different scroll compressors, one with the possibility to use vapor injection and speed control (CEV), and one with constant-speed (CSD), are chosen. For the first compressor measured efficiency data from a test rig (chapter 3) is used for the described heat pump model. For the second compressor manufacturer data is used. Both compressors are considered for the comparison of the dynamic system simulation in chapter 4 and their technical data is provided in Table 2.

Table 2: Technical data of the considered scroll compressors, with economizer and variable speed control (CEV) and constant-speed control only (CSD)

compressor		CEV	CSD
Swept volume (V_{swept})	ccm	15.56	49.44
Speed range	rpm	1800 - 7020	3000 only
Refrigerant		R410A	R410A
Heating capacity at t_{evap} = -15 °C & t_{cond} = 55 °C; ΔT_{sup} = 5 K, ΔT_{sub} = 0 K	kW	8.6	8.9

Both compressors meet the heating load of the building plus additional 0.5 kW for DHW preparation. In case of the CSD the capacity (8.9 kW) is only slightly higher compared to the CEV (8.6 kW) since the compressor data is based on real compressors.

3 EXPERIMENTAL ANALYSIS AND VALIDATION OF THE HEAT PUMP MODEL

This chapter deals with the description of the heat pump test rig with CEV and its measurement points, discusses the uncertainty of measurements on the basis of Gaussian uncertainty propagation, provide information for the determined compressor efficiencies $\eta_{is,over}$ and η_{vol} as well as $\dot{Q}_{comp,loss}$, which are used as input for the heat pump model and afterwards the validation of the heat pump model, which is considered in the dynamic simulation model.

Figure 3 depicts the refrigerant cycle layout of the heat pump test rig with the used measurement equipment. In addition to the already described economizer cycle the test rig allows to use a desuperheater for DHW preparation. However, this was not considered in the simulations described in this work.

Table 3 shows a list of the measuring equipment and accuracies. With the information of the table the measurement errors are calculated for each measuring point. For instance the calculated COP (on the water-side of the condenser) by means of the measurements at t_{evap} = -16.13 °C, t_{cond} = 26.6 °C and n_{comp} at 3600 rpm is about 3.8 ±0.033 (±0.87 %)[1].

At the hermetic compressor with vapor injection only the inlet conditions at the two suction ports (evaporation and intermediate pressure) and the outlet conditions at the discharge line can be measured. For the determination of $\eta_{is,over}$ it is assumed, that $\eta_{is,over}$ is the same for the lower and higher pressure stage. Formula (1) represents $\eta_{is,over}$ for both pressure stages, which is determined from the experimental data. $P_{is,lp}$ represents the isentropic compression of the low pressure stage and $P_{is,hp}$ of the high pressure stage. To determine $\eta_{is,over}$ both isentropic compressions are summed up and related to the overall electric power consumption of the compressor plus inverter $P_{el,comp}$.

η_{vol} is determined separately for the lower pressure stage and the high pressure stage also using the experimental data from the test rig. Formula (2) shows $\eta_{vol,lp}$ for the volumetric efficiency at the low pressure compression and $\eta_{vol,hp}$ for the high pressure compression of the compressor. In case of the volumetric efficiency the separate determination can be done because of the described simplification concerning $\eta_{is,over}$, which allows a determination of the inlet condition for the second compressor stage. The factor $f_{comp,size,hp}$ is also obtained from the measurements and describes the swept volume of the high pressure part in relation to the swept volume of the low pressure part of the compressor.

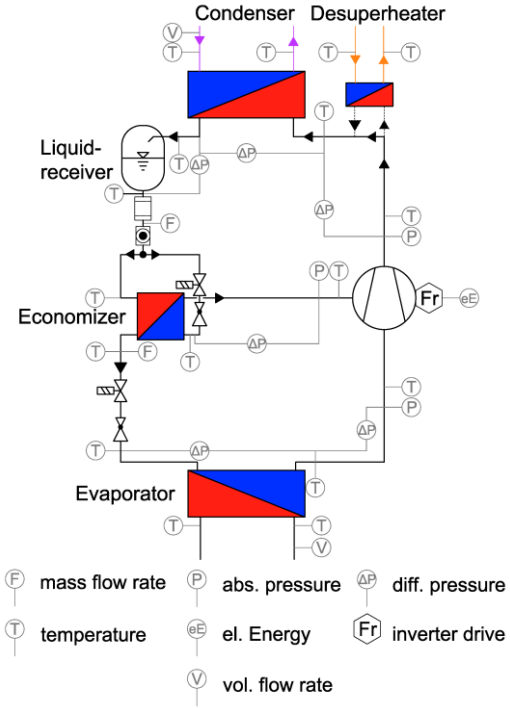

Figure 3: Refrigerant cycle layout of the heat pump test rig

Figure 4 depicts the measurement results of the compressor from the CEV test rig for $\eta_{is,over}$ and η_{vol} depending on the pressure ratio π_{comp} (formula (3)) and the

[1] measurement error calculated according to Gaussian uncertainty propagation

compressor speed n_{comp} and additionally $\eta_{is,over}$ and η_{vol} depending also on π_{comp} for CSD by means of the manufacturer data.

Table 3: Type, measuring range and accuracy of the used sensors in the heat pump test rig

	temperature source / sink side	temperature ref-side	vol. flow rate	mass flow rate	el. energy	abs. pressure	diff. pressure
Type	Pt100	TC type K	Magnetic inductive	Coriolis	Pulse counter	Resistance strain gauge	capa-citive
Calibration range	-20 to +90 °C	-20 to +90 °C	0 to 1200 kg/h	0 to 130 kg/h	0 to 4.6 kW AC	0 to 20 0 to 30 0 to 50 bar	0 to 1000 mbar
max error (calibrated)	±0.02 K	±0.2 K	±1 %	±0.3 %	Class B[2]	±0.02 %[3]	FSO ±0.1 %

$$\eta_{is,over} = \frac{\left(P_{is,hp} + P_{is,lp}\right)}{P_{el,comp}} \quad (1)$$

$$\eta_{vol,lp} = \frac{\dot{m}_{ref,lp} \cdot v_{ref,lp}}{\dot{V}_{swept}} \quad and \quad \eta_{vol,hp} = \frac{\dot{m}_{ref,hp} \cdot v_{ref,ip}}{\dot{V}_{swept} \cdot f_{comp,size,hp}} \quad (2)$$

$$\pi_{comp} = \frac{p_{cond}}{p_{evap}} \quad (3)$$

In case of $\eta_{is,over}$ the measured data shows results from 0.64 to 0.48. The highest value is reached at a n_{comp} of about 4800 rpm to 5400 rpm at rather low pressure ratios ($\pi_{comp} \cong 3$). The lowest values for $\eta_{is,over}$ are measured at the lowest considered compressor speed (2100 rpm). At all n_{comp} the max. of $\eta_{is,over}$ occurs at $\pi_{comp} \cong 3$. η_{vol} (Figure 4, right side) shows a typical behavior, it decreases (almost) linearly with increasing pressure ratio.

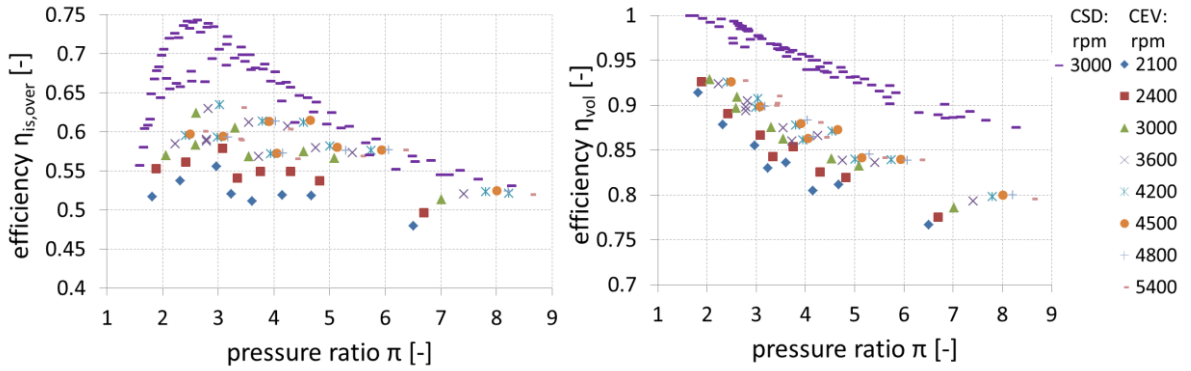

Figure 4: Experimental data for $\eta_{is,over}$ (left) and for η_{vol} (right) for the speed controlled compressor with vapor injection

A little degradation of η_{vol} can be observed for n_{comp} of 2100 rpm and 2400 rpm. This confirms the hypothesis of internal leakages at low compressor speeds.

[2] class B according to IEC 50470-3 or (1%) according to IEC 62053-21
[3] calibrated from 5 to 20 bar for low pressure, 10 to 30 bar for intermediate pressure and 20 to 50 bar for high pressure

The compressor heat loss $\dot{Q}_{comp,losses}$ is determined by means of the energy balance over the whole compressor, which is shown in formula (4), where the first term represents the conditions at the inlet of the compressor on the low pressure stage, the second term the inlet conditions at the injection port at the intermediate pressure and the third term considers the electric power consumption of the compressor and inverter. The last term provides the outlet conditions of the compressor on the high pressure stage.

$$\dot{Q}_{comp,losses} = \dot{m}_{ref,lp} \cdot h_{ref,lp} + \dot{m}_{ref,inj} \cdot h_{ref,ip} + P_{el,comp} - \dot{m}_{ref,hp} \cdot h_{ref,hp} \quad (4)$$

Figure 5 shows the compressor heat losses $\dot{Q}_{comp,losses}$ as a percentage of $P_{el,comp}$. The heat losses $f_{comp,losses}$ increase in an approximately linear way with increasing pressure ratio. The deviations between the compressor speeds of 5400 rpm to 3000 rpm are relative low. Only at n_{comp} of 2100 rpm and 2400 rpm the deviation to the higher compressor speeds is higher, where the highest factor is reached at the lowest compressor speed. Additionally, the results from manufacturer data for CSD show $f_{comp,losses}$ between 4 % and 7 %.

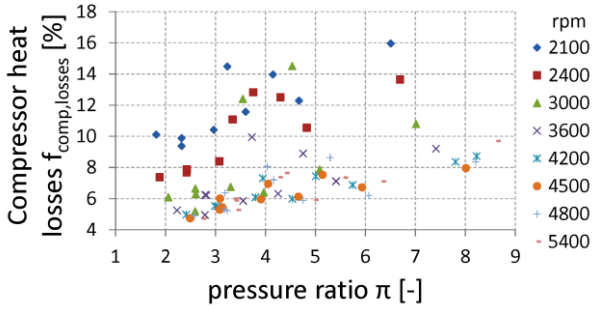

Figure 5: Experimental data for $f_{comp,losses}$ for the speed controlled compressor with vapor injection

The obtained measurement results are used to generate polynomials for $\eta_{is,over}$ and η_{vol} as well as for $\dot{Q}_{comp,losses}$ of the compressor, which depend on t_{evap} (-19 °C to +7 °C), t_{cond} (+23 °C to 62 °C) and n_{comp} (2100 rpm to 5400 rpm).

With these polynomials as input for the heat pump model (chapter 2.3) a validation was carried out with the heating capacity of the condenser $\dot{Q}_{cond}$ and the coefficient of performance COP (Figure 6).

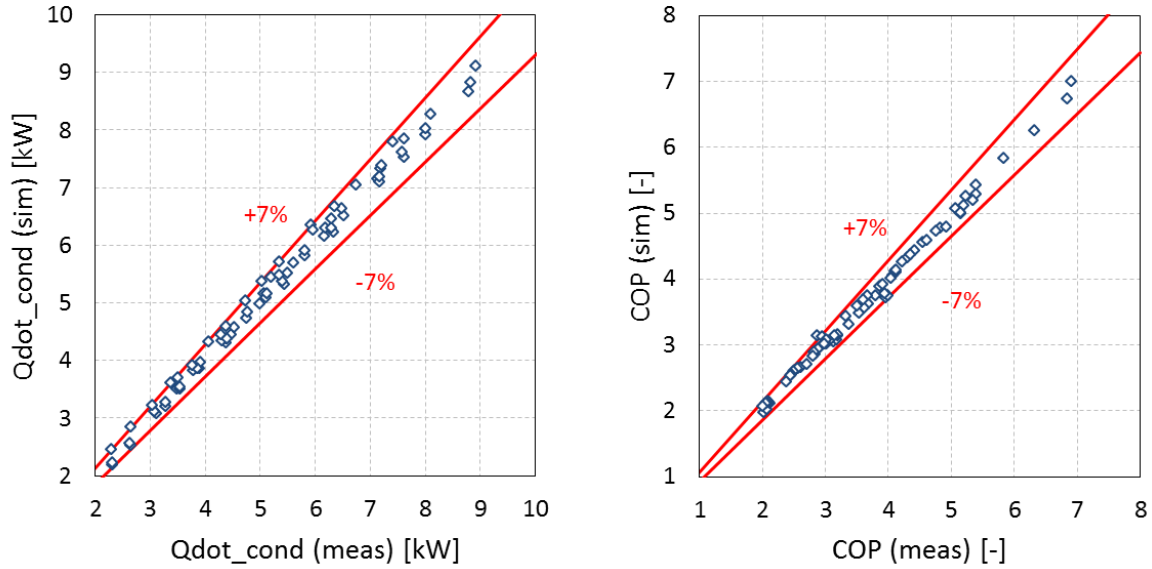

Figure 6: Simulation results vs. experimental data for the CEV test rig

The results of the heat pump model show slightly higher values for $\dot{Q}_{cond}$ and for COP compared to the experimental data. This is mainly due to the non-consideration of the pressure drop within the heat exchangers, especially in the evaporator. Hence the evaporation temperature is slightly lower in the measurements compared to the simulation

results, but COP and $\dot{Q}_{cond}$ stay within a tolerance of ±7 % between measurements and simulations. With this validated model the annual dynamic system simulations are carried out in chapter 4.

4 RESULTS AND DISCUSSION

This chapter shows the results of the dynamic system simulations with the validated heat pump model using speed controlled compressor and economizer cycle (CEV) and on the other hand the modelled heat pump using a constant-speed compressor with manufacturer data (CSD). Within the system simulation the dynamic processes - especially the interaction between heat pump system and hydronic system as well as the start and stop losses of the heat pump – are considered.

To compare both systems the following key figures are defined (formula (5) to (7)).

$$P_{el,sys} = P_{el,hp} + P_{el,pu} + P_{el,ctr} \tag{5}$$

$$COP = \frac{P_{cond}}{P_{el,hp}} \tag{6}$$

$$SPF_{sys} = \frac{\int_{\tau=0}^{8760h} \left(\dot{Q}_{sh} + \dot{Q}_{DHW}\right) \cdot d\tau}{\int_{\tau=0}^{8760h} \left(P_{el,sys}\right) \cdot d\tau} \tag{7}$$

The results of the dynamic system simulation for the standard heat pump cycle (CSD) show a seasonal performance factor SPF_{sys} of 2.63 and an annual electric energy consumption $W_{el,sys}$ of 9395 kWh. SPF_{sys} can be increased by about 14.8 %, corresponding to electric energy savings of about 13.5 %, with the advanced heat pump cycle CEV. This is mainly due to lower water outlet temperatures at the condenser that are reached due to the speed control and the economizer cycle (compare Figure 7). The latter can be explained by the fact that the heating capacity of the CEV does not increase to the same extent as that of the CSD with increasing ambient temperatures, which is due to a decreasing injection mass flow rate at lower pressure ratios.

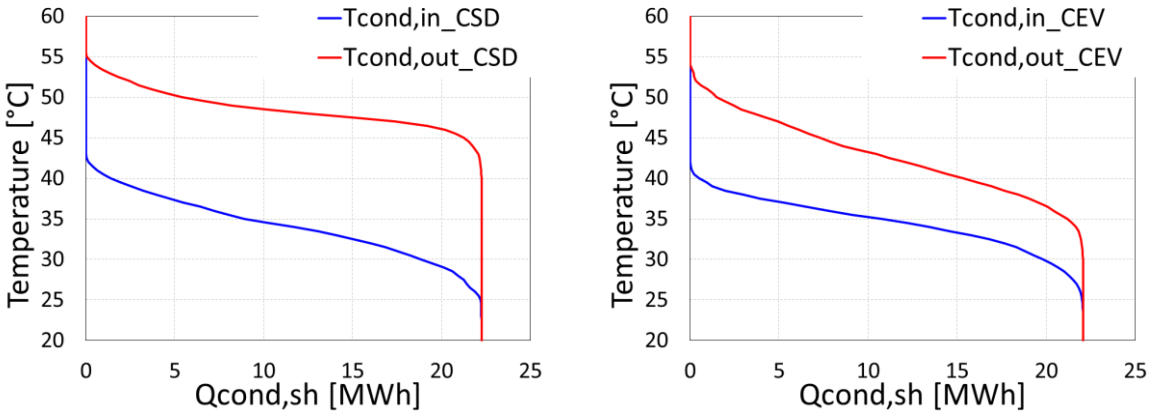

Figure 7: Heat provided by the heat pump condenser with different inlet and outlet water temperatures; left: without speed control, right: with speed control

Figure 7 depicts on the left side the condenser inlet and outlet water temperatures over the provided energy of the heat pump for space heating for CSD and on the right side for CEV. It can be observed that by using the CEV system the temperature at the outlet of the condenser is lower than the temperature of the CSD. Hence, the condensation temperature of the CSD system is higher than for the CEV system which does have a degradation effect on the COP.

Another reason is the reduction of starting losses of the heat pump. This is mainly due to lower numbers of starts for CEV compared to the CSD, which is mainly a result of the compressor speed control and its lower heating capacities at higher ambient temperatures. In case of CSD the heating capacity increases with increasing of the ambient temperature but cannot be totally compensated by the storage (too small) in the return line, so the numbers of starts are higher for the CSD. Table 4 shows detailed information for both heat pump systems, e.g. number of heat pump starts (HP starts), the average runtime per start of the heat pumps, the electric energy consumption of the fan $W_{el,fan}$ and the circulation pump $W_{el,pu}$ as well as the starting heat losses $Q_{start,losses}$. The consumption of the circulation pumps of both systems (CEV and CSD) is nearly equal because the pumps for space heating are constantly running during the heating season. This is necessary for the used control strategy (heat pump status on/off by means of the return line temperature) and on the other hand the influence of the total electric energy consumption is lower than 0.6 % for both systems.

Table 4: Detailed information of both heat pump systems (CEV and CSD)

System	SPF_{sys}	HP starts	avg. runtime per start	$W_{el,sys}$	$W_{el,fan}$	$W_{el,pu}$	$Q_{start,losses}$
	[-]	[-]	[h]	[kWh/a]	[kWh/a]	[kWh/a]	[kWh/a]
CEV	3.02	1457	4.5	8133	991	48	452
CSD	2.63	3354	1.2	9395	600	48	880

5 SUMMARY

This paper presents the analysis of a heat pump for a retrofit building with 154 kWh/(m²·a) and a radiator space heating system equipped with a scroll compressor with vapor injection (economizer cycle with plate heat exchanger) and speed control (CEV) in comparison to a heat pump with a “standard” compressor (CSD).

The compressor analysis provided a detailed view about the compressor efficiencies, overall isentropic efficiency and volumetric efficiency as well as the compressor heat losses at different compressor speeds and different pressure ratios by means of experimental data for CEV.

The performed compressor analysis showed the compressor efficiencies and the heat losses of a CEV. It could be seen that a max. for $\eta_{is,over}$ occurs at a pressure ratio of about three for all compressor speeds. Left and right of the maximum the efficiency is decreasing where the lowest compressor speed leads to the lowest efficiency. Also for the volumetric efficiency the lowest efficiency occurs at the lowest n_{comp}. As expected the volumetric efficiency decreases linearly with increasing pressure ratio for all compressor speeds.

The results of the compressor heat losses based on the electric power of the compressor shows that the highest loss occurs at the lowest n_{comp} and the highest pressure ratio. For higher compressor speeds the deviation is small. In general, the heat losses increase with increasing pressure ratio.

With the obtained experimental data a simulation model has been fitted. Here, especially the overall isentropic efficiency, the volumetric efficiency for both pressure stages and the heat losses of the compressor were used to generate polynomial performance maps as input to the simulation heat pump model.

With the generated polynomials for the model a validation of the heat pump simulation model was carried out with the measurements, which showed a maximum deviation of ±7 % for the heating capacity and the COP. With the validated model two different systems, CEV and CSD, were compared by means of dynamic annual system simulations under defined boundary conditions.

In annual dynamic system simulations a heat pump with CEV and a heat pump with CSD were compared assuming the same hydronic system and the same boundary conditions. The results of these simulations show a higher efficiency for the advanced heat pump system (CEV), and an increase in SPF_{sys} of about 14.8 % as well as an electric energy saving of about 13.5 % although the electric energy consumption of the heat pump ventilator is higher for the advanced heat pump system due to longer runtimes of the heat pump. Another reason for the higher efficiency of the CEV is the lower water outlet temperature at the condenser at lower pressure ratios, this is mainly due to the speed controlled compressor (compare Figure 7) and due to the advantages of the economizer cycle in case of higher pressure ratios (compare Figure 2). The advanced heat pump cycle also achieves a reduction of the start and stop losses of more than 50 % compared to CSD.

It can be stated that there is a large energy saving potential, if an advanced heat pump cycle with an economizer and a speed controlled compressor is used instead of a fixed speed “standard” compressor.

6 NOMENCLATURE

Nomenclature		Subscripts	
CEV	heat pump with economizer and speed controlled compressor	$comp$	compressor
COP	coefficient of performance for heating	$cond$	condenser
CSD	heat pump with constant-speed compressor	ctr	control devices
EVI	heat pump with enhanced vapor injection	DHW	domestic hot water
f	factor	el	electric
h	specific enthalpy [kJ/(kg·K)]	hp	heat pump or high pressure
$\dot{m}$	mass flow rate [kg/s]	inj	injection
n	speed [rpm]	ip	intermediate pressure
P	power [kW]	is	isentropic
p	pressure [bar]	$loss$	heat losses
$\dot{Q}$	heat transfer rate [kW]	lp	low pressure
SPF	seasonal performance factor	$over$	overall
t	temperature [°C]	pu	circulation pump
$\dot{V}$	volumetric flow rate [m³/h]	ref	refrigerant-side
VSD	heat pump with speed controlled compressor	rt	return line
		set	set point
Greek symbols		sh	space heating
π	pressure ratio [-]	sys	system
η	compressor efficiency [-]	$swept$	swept volume of the compressor
τ	time [s]	v	volumetric
		ww	warm water

7 REFERENCES

Afjei, T., Schonhardt, U., Wemhöner, C., Erb, M., Gagathuler, H.R., Mayer, H., Zweifel, G.; Achermann, M., von Euw, R., Stöckli, U., 2002. "Standardschaltungen für Kleinwärmepumpenanlagen – Teil 2: Grundlagen und Computersimulationen", final report, Bundesamt für Energie, Switzerland.

Aprea, C., Mastrullo, R., Renno, C. & Vanoli, G.P., 2004. "An evaluation of R22 substitutes performances regulating continuously the compressor refrigeration capacity", Applied Thermal Engineering, 24(1), pp.127–139.

Bales, C., Heinz, A., Haller, M., 2012. „Definition of Boundary Conditions", European Union's Seventh Framework Programme FP7/2007-2011 No. 282825 - Acronym "MacSheep", internal document.

Bertsch, S.S. and Groll, E.A., 2008. "Two-stage air-source heat pump for residential heating and cooling applications in northern U.S. climates", International Journal of Refrigeration, 31(7), pp.1282–1292.

Cuevas, C. and Lebrun, J. 2009. "Testing and modelling of a variable speed scroll compressor", Applied Thermal Engineering, 29 (2-3), pp. 469 – 478.

Gasser, L., Wellig, B. & Hilfiker, K., 2008. "WEXA: Exergie-Analyse zur Effizienzsteigerung von Luft/Wasser-Wärmepumpen", final report, Bundesamt für Energie, Switzerland.

Heinz, A., Haller, M., 2012. Appendix A3 - Description of TRNSYS Type 877 by IWT and SPF. In: Models of Sub-Components and Validation for the IEA SHC Task 44 / HPP Annex 38 - Part C: Heat Pump Models - DRAFT - A technical report of subtask C Deliverable C2.1 Part C.

Heo, J., Jeong, M.W., Baek, C. & Kim, Y., 2011. "Comparison of the heating performance of air-source heat pumps using various types of refrigerant injection", International Journal of Refrigeration, 34(2),pp.444–453.

Liegeois, O. & Winandy, E., 2008. "Scroll Compressors for Dedicated Heat Pumps: Development and Performance Comparison", International Compressor Engineering Conference, Paper 1906, Purdue e-Pubs, Purdue University, Indiana, USA.

Streicher, W., Heimrath, R., 2003. "Structure of the Reference Buildings of Task 26, A Report of IEA SHC – TASK 26 Subtast C: Solar Combisystems", 2003.

SWEP, 2014. http://www.swep.net/de/Pages/default.aspx accessed on 06.02.2014 at 13:00.

TRNSYS, 2012. "A transient system simulation program", Version v17.01.0016, Solar Energy Laboratory, University of Wisconsin, Madison.

8 Acknowledgement

The research leading to these results has received funding from the European Union's Seventh Framework Programme FP7/2007-2011 under grant agreement nº 282825 – Acronym MacSheep.